Investigating the association between late spring Gulf of Mexico sea surface temperatures and US Gulf Coast precipitation extremes with focus on Hurricane Harvey

Brook T. Russell* Mark D. Risser † Richard L. Smith ‡

Ken Kunkel § ¶

July 23, 2019

Keywords: Multivariate spatial modeling; Generalized Extreme Value distribution; Precipitation return levels; Covariance tapering; Coregionalization

Abstract

Hurricane Harvey brought extreme levels of rainfall to the Houston, TX area over a seven-day period in August 2017, resulting in catastrophic flooding that caused loss of human life and damage to personal property and public infrastructure. In the wake of this event, there has been interest in understanding

*Clemson University Department of Mathematical Sciences, Clemson, SC 29634 (email: brookr@clemson.edu, office: 864-656-4571, fax: 864-656-5230)

†Lawrence Berkeley National Lab, Berkeley, CA 94720

‡University of North Carolina–Chapel Hill Department of Statistics and Operations Research, Chapel Hill, NC 27599

§North Carolina State University Department of Marine, Earth, and Atmospheric Sciences, Raleigh, NC 27695

¶Cooperative Institute for Climate and Satellites–NC, Asheville, NC 28801

the degree to which this event was unusual and estimating the probability of experiencing a similar event in other locations. Additionally, researchers have aimed to better understand the ways in which the sea surface temperature (SST) in the Gulf of Mexico (GoM) is associated with precipitation extremes in this region. This work addresses all of these issues through the development of a multivariate spatial extreme value model.

Our analysis indicates that warmer GoM SSTs are associated with higher precipitation extremes in the western Gulf Coast (GC) region during hurricane season, and that the precipitation totals observed during Hurricane Harvey are less unusual based on the warm GoM SST in 2017. As SSTs in the GoM are expected to steadily increase over the remainder of this century, this analysis suggests that western GC locations may experience more severe precipitation extremes during hurricane season.

1 Introduction

Hurricane Harvey brought massive amounts of rainfall to the Houston, Texas area from August 25–31, 2017. Over that seven-day period, portions of Houston were inundated with precipitation totals approaching 80 cm, leading to flooding that resulted in loss of life and damage to property. As this disastrous and highly impactful event came to an end, important questions came to the forefront; in this work, we attempt to address some of these issues. To this end, we aim to characterize the degree to which the Harvey event was anomalous and to estimate the probability of observing additional precipitation events of this magnitude in the Gulf Coast (GC) region, while taking into account the impact of sea surface temperatures (SSTs) in the Gulf of Mexico (GoM).

Extreme value theory (EVT), the branch of statistics that models the far upper

tails of the distributions of random variables, offers approaches that may be useful for modeling precipitation events such as Harvey. In the US GC region, the series of precipitation observations at individual stations is relatively short, and estimators used to characterize extremes may have a relatively high degree of uncertainty associated with them. Therefore, in order to reduce uncertainty by borrowing strength from nearby locations, we utilize a spatial modeling procedure; the ultimate goal in this work is to address our research aims via a spatial model built within the framework provided by EVT.

Davison et al. (2012) and Cooley et al. (2012) offer overviews of spatial extremes methods and highlight several popular modeling approaches, including max-stable process models and latent process models. Max-stable processes (Brown and Resnick, 1977; Opitz, 2013; Kabluchko et al., 2009; Ribatet and Sedki, 2013; Schlather and Tawn, 2003; Smith, 1990) yield models that are theoretically appealing and have the ability to model the spatial extent of extreme events; however, the likelihood is not tractable for even a relatively small number of stations and therefore inference is less than straightforward. If the primary focus of the analysis is on marginal quantities, such as pointwise return levels or exceedance probabilities, latent process models are often preferred. In these models, the parameters of a univariate extreme value distribution, such as the Generalized Extreme Value (GEV) distribution or the Generalized Pareto Distribution (GPD), are assumed to be realizations of latent spatial processes; for inference, Bayesian approaches are often utilized. For example, Cooley et al. (2007) use a Bayesian hierarchical modeling approach to spatially model GPD parameters across a large portion of Colorado. Other works have used Bayesian hierarchical approaches to spatially model GEV parameters (Cooley and Sain, 2010; Dyrrdal et al., 2015; Gaetan and Grigoletto, 2007; Ghosh and Mallick, 2011; Schliep et al., 2010; Sang and Gelfand, 2009).

In the modeling approach taken in this work, we assume that maximum seven-day precipitation totals during hurricane season at GC locations approximately follow the GEV distribution. In order to investigate the ways in which the SST in the GoM is associated with extreme precipitation in the US GC, we allow these GEV parameters to depend on a GoM SST covariate. Exploratory analysis suggests that there may be dependence among GEV parameters, and therefore we develop a multivariate spatial model; for inference, a two-stage frequentist approach is employed. Other works have used similar two-stage inference approaches in spatial analyses (Holland et al., 2000; Russell et al., 2016; Tye and Cooley, 2015). Nearby locations may experience extreme precipitation from the same event, resulting in dependence between annual maxima for which many previous spatial models of this sort have failed to account. Our model allows us to incorporate dependence of this type and uses the nonparametric bootstrap to estimate its effect. Spatial interpolation is used to estimate GEV parameters at unobserved locations, allowing us to characterize precipitation extremes throughout the GC region.

Immediately following Hurricane Harvey, several works analyzed the event and its impact on the region. Risser and Wehner (2017) model precipitation extremes in the Houston area via the GEV distribution and conclude that human induced climate change was likely responsible for at least an 18.8% precipitation increase in the Harvey event, and likely increased the chances of seeing that level of observed rainfall by a factor of at least 3.5. The analysis of van Oldenborgh et al. (2017) uses comparisons of GEV fits to extreme precipitation on both observational and model data to perform an attribution analysis. They conclude that global warming made Harvey precipitation approximately 15% more intense and also made an event of Harvey's magnitude three times more likely to occur. The approach of Emanuel (2017) is based on simulating a large number of GC storms using an atmospheric model with boundary conditions

taken from general circulation models (GCMs), allowing him to make projections for future extreme events by using boundary conditions from GCMs under projected future scenarios. Based on this analysis, he estimates the chances of observing an event of Harvey's magnitude in the present and in the future, and predicts a sharp increase in this probability under global warming scenarios. Trenberth et al. (2018) also take a physical based modeling approach, and investigate the link between oceanic warming and Hurricane Harvey. The work concludes that warmer ocean temperatures provided additional energy that resulted in higher precipitation levels for Harvey. All of the works mentioned here provide insight and analysis that help to better understand the Harvey event and the ways in which it may be related to climate change; however, the analysis provided in this work is fundamentally different in terms of the modeling procedure and research aims. We aim to utilize a spatial analysis to understand precipitation extremes over for a larger spatial domain. Emanuel (2017) does give some results for the whole GC region, but he did not provide a methodology for observing how probabilities of extreme events vary over that region, which this paper does.

This manuscript is organized in the following manner. Section 2 begins by giving a brief review of univariate extremes and the block maxima approach; it concludes by introducing our multivariate spatial model and two-step inference procedure. Section 3 describes the data used in this work, and presents the results of the multivariate spatial analysis with focus on the role that GoM SST plays on GC precipitation extremes. We conclude with a discussion in Section 4, where we consider the impact of SST projections on precipitation extremes in the region.

2 Background and Modeling Procedure

We begin this section by reviewing the GEV distribution and the block maxima approach from univariate EVT. We then describe our multivariate spatial model and our corresponding two-stage frequentist inference procedure. Next, we describe our method of accounting for dependence between annual maxima at nearby locations, and conclude by outlining our method for spatial interpolation.

2.1 Block Maxima Approach to Univariate Extremes

In EVT, the block maxima approach provides a theoretical framework for univariate extreme value analysis, and is an commmon choice for modeling the far upper tail of pointwise precipitation data. Define $M_n = \text{Max}\{X_1, \ldots, X_n\}$ for the iid sample $X_1, \ldots, X_n$. If there exist sequences $a_n > 0$ and b_n such that

$$P\left(\frac{M_n - b_n}{a_n} \leq z\right) \to G(z)$$

for non-degenerate G, then G must be a member of one of the following families: Reversed Weibull, Gumbel, or Fréchet. The Generalized Extreme Value (GEV) distribution is a three parameter family that contains each of the three aforementioned distributions as a special case. For $Z \sim \text{GEV}(\mu, \sigma, \xi)$, its cumulative distribution function is defined by

$$P(Z < z) = \exp\left(-\left(1 + \xi\left(\frac{z-\mu}{\sigma}\right)\right)_+^{-1/\xi}\right), \tag{1}$$

where $c_+ := \max\{c, 0\}$. The GEV parameters are typically referred to as the *location* parameter $\mu \in \mathbb{R}$, the *scale* parameter $\sigma > 0$, and the *shape* parameter $\xi \in \mathbb{R}$. The shape parameter characterizes the GEV density's tail: when $\xi < 0$, the tail will be

bounded and the GEV reduces to the Reversed Weibull; for $\xi > 0$, the tail is heavy and the GEV reduces to the Fréchet; and $\xi \to 0$ results in a light tail, and the GEV is equivalent to the Gumbel. The reader is referred to Coles (2001) as an introductory resource for univariate extremes.

The three GEV parameters can be used to characterize extremes through summary parameters, some of which are determined by the quantile function of the GEV. For $Z \sim \text{GEV}(\mu, \sigma, \xi)$, the value that is exceeded with probability $p \in (0, 1)$ can be calculated via

$$Z_p(\mu, \sigma, \xi) = \begin{cases} \mu - \frac{\sigma}{\xi}(1 - \{-\log(1-p)\}^{-\xi}) \text{ for } \xi \neq 0 \\ \mu - \sigma \log\{-\log(1-p)\} \text{ for } \xi = 0. \end{cases} \tag{2}$$

When the data are structured such that each year contains exactly one block, the r-year return level is given by $RL_r = Z_p(\mu, \sigma, \xi)$ for $p = r^{-1}$.

For inference, the GEV parameters are typically estimated based on a sample of block maxima using a likelihood or moment based method (Coles, 2001). Based on the resulting GEV parameter estimates, the r-year return level can be estimated via $\widehat{RL}_r = Z_{r^{-1}}(\hat{\mu}, \hat{\sigma}, \hat{\xi})$ using Eq. (2). Another useful quantity to estimate is the probability of observing a block maximum that exceeds some value of interest, z'. This exceedance probability, $P(Z > z')$, can be estimated using Eq. (1) based on the parameter estimates $\hat{\mu}$, $\hat{\sigma}$, and $\hat{\xi}$.

2.2 Multivariate Spatial Model

For $Y_t(\boldsymbol{s})$, the seasonal 7-day maximum precipitation total in year t at location $\boldsymbol{s} \in \mathcal{D} \subset \mathbb{R}^2$, assume

$$Y_t(\boldsymbol{s}) \dot{\sim} \text{GEV}(\mu_t(\boldsymbol{s}), \sigma_t(\boldsymbol{s}), \xi(\boldsymbol{s})).$$

In order to investigate the relationship between precipitation extremes in the US Gulf Coast region and GoM SST, we incorporate an annual GoM SST covariate in year t into the location and scale parameters by modeling the parameters of the GEV at location $\boldsymbol{s}$ via

$$\begin{aligned} \mu_t(\boldsymbol{s}) &= \theta_1(\boldsymbol{s}) + SST_t\ \theta_2(\boldsymbol{s}) \\ \log \sigma_t(\boldsymbol{s}) &= \theta_3(\boldsymbol{s}) + SST_t\ \theta_4(\boldsymbol{s}) \\ \xi(\boldsymbol{s}) &= \theta_5(\boldsymbol{s}). \end{aligned} \tag{3}$$

In univariate extremes, the shape parameter is known to be the most difficult parameter to estimate; therefore, we choose not to include SST in its functional form.

To allow us to characterize precipitation extremes throughout the region, a primary aim of this work is to be able to estimate these parameters $\forall\ \boldsymbol{s} \in \mathcal{D}$, observed and unobserved. To this end, we rely on a multivariate spatial model. At location $\boldsymbol{s} \in \mathcal{D}$ and $\boldsymbol{\theta}(\boldsymbol{s}) = (\theta_1(\boldsymbol{s}), \theta_2(\boldsymbol{s}), \theta_3(\boldsymbol{s}), \theta_4(\boldsymbol{s}), \theta_5(\boldsymbol{s}))^T$, we assume

$$\boldsymbol{\theta}(\boldsymbol{s}) = \boldsymbol{\beta} + \boldsymbol{\eta}(\boldsymbol{s}) \tag{4}$$

where $\boldsymbol{\beta} = (\beta_1, \beta_2, \beta_3, \beta_4, \beta_5)^T$ represents the mean parameter values over $\mathcal{D}$ and $\boldsymbol{\eta}(\boldsymbol{s}) = (\eta_1(\boldsymbol{s}), \eta_2(\boldsymbol{s}), \eta_3(\boldsymbol{s}), \eta_4(\boldsymbol{s}), \eta_5(\boldsymbol{s}))^T$ are spatially correlated random effects. In order to obtain a relatively simple multivariate spatial model, we use the coregionalization formulation (Wackernagel, 2003),

$$\boldsymbol{\eta}(\boldsymbol{s}) = A\ \boldsymbol{\delta}(\boldsymbol{s}), \tag{5}$$

for $\boldsymbol{\delta}(\boldsymbol{s}) = (\delta_1(\boldsymbol{s}), \delta_2(\boldsymbol{s}), \delta_3(\boldsymbol{s}), \delta_4(\boldsymbol{s}), \delta_5(\boldsymbol{s}))^T$ and lower triangular matrix A. The lower

triangular formulation is suggested by Finley et al. (2008) and δ_i ($i \in \{1, \ldots, 5\}$) are independent second-order stationary Gaussian processes with mean 0 and covariance function given by $Cov(\delta_i(\boldsymbol{s}), \delta_i(\boldsymbol{s}')) = \exp(-\|\boldsymbol{s} - \boldsymbol{s}'\|/\rho_i)$ for $\boldsymbol{s}, \boldsymbol{s}' \in \mathcal{D}$, where $\rho_i > 0$ is the range parameter. In this work, we exclusively utilize the exponential covariance function as we believe that use of alternative covariance functions would make little difference in terms of estimating $\boldsymbol{\theta}(\boldsymbol{s})$ at $\boldsymbol{s} \in \mathcal{D}$, which is ultimately the purpose of the analysis. This issue has been addressed in prior literature, and the results show that choice of spatial covariance function makes little difference in the predictions of interest (Holland et al., 2000, 2004).

2.3 Two-Stage Inference Procedure

At the first stage of inference, we obtain pointwise maximum likelihood estimates $\hat{\boldsymbol{\theta}}(\boldsymbol{s}_l) = (\hat{\theta}_1(\boldsymbol{s}_l), \hat{\theta}_2(\boldsymbol{s}_l), \hat{\theta}_3(\boldsymbol{s}_l), \hat{\theta}_4(\boldsymbol{s}_l), \hat{\theta}_5(\boldsymbol{s}_l))^T$ at station $l \in \{1, \ldots, L\}$. We then make the assumption that

$$\hat{\boldsymbol{\theta}}(\boldsymbol{s}_l) = \boldsymbol{\theta}(\boldsymbol{s}_l) + \boldsymbol{\varepsilon}(\boldsymbol{s}_l), \tag{6}$$

where $\boldsymbol{\varepsilon}(\boldsymbol{s}_l) = (\varepsilon_1(\boldsymbol{s}_l), \varepsilon_2(\boldsymbol{s}_l), \varepsilon_3(\boldsymbol{s}_l), \varepsilon_4(\boldsymbol{s}_l), \varepsilon_5(\boldsymbol{s}_l))^T$ is estimation error that is independent of $\boldsymbol{\eta}$. Equations (4), (5), and (6) imply

$$\hat{\boldsymbol{\theta}}(\boldsymbol{s}_l) = \boldsymbol{\beta} + A\ \boldsymbol{\delta}(\boldsymbol{s}_l) + \boldsymbol{\varepsilon}(\boldsymbol{s}_l).$$

We further assume that

$$(\varepsilon_1(\boldsymbol{s}_1), \ldots, \varepsilon_1(\boldsymbol{s}_L), \ldots, \varepsilon_5(\boldsymbol{s}_1), \ldots, \varepsilon_5(\boldsymbol{s}_L))^T \sim N(\mathbf{0}, \boldsymbol{W}),$$

where $\mathbf{0}$ is the zero vector and $\boldsymbol{W}$ is an unknown covariance matrix. This multivariate Gaussian assumption is justified by asymptotic theory for maximum likelihood

estimators (MLE). Even in the dependent case, the CLT for the score statistic (the first derivative vector for the log likelihood) implies multivariate Normality in large samples. This is then normalized by the inverse of the Fisher information matrix, leading to multivariate Normality for the MLE. This argument is valid in any case where the usual regularity conditions for MLE apply.

Defining

$$\boldsymbol{\Theta} = (\theta_1(\boldsymbol{s}_1), \ldots, \theta_1(\boldsymbol{s}_L), \ldots, \theta_5(\boldsymbol{s}_1), \ldots, \theta_5(\boldsymbol{s}_L))^T$$

and

$$\hat{\boldsymbol{\Theta}} = (\hat{\theta}_1(\boldsymbol{s}_1), \ldots, \hat{\theta}_1(\boldsymbol{s}_L), \ldots, \hat{\theta}_5(\boldsymbol{s}_1), \ldots, \hat{\theta}_5(\boldsymbol{s}_L))^T,$$

we obtain the model

$$\hat{\boldsymbol{\Theta}} \sim N(\boldsymbol{\beta} \otimes \mathbf{1}_L, \boldsymbol{\Sigma}_{A,\boldsymbol{\rho}} + \boldsymbol{W}) \tag{7}$$

for

$$\boldsymbol{\Sigma}_{A,\boldsymbol{\rho}} := (\boldsymbol{I}_L \otimes A) \left[\sum_{i=1}^{5} \left(\boldsymbol{e}_i \boldsymbol{e}_i^T \otimes \ \boldsymbol{\Omega}_i(\boldsymbol{\rho}) \right) \right] (\boldsymbol{I}_L \otimes A)^T,$$

where $\otimes$ represents the Kronecker product, $\boldsymbol{I}_L$ is the L dimensional identity matrix, $\mathbf{1}_L$ is a vector of ones having length L, $\boldsymbol{e}_i$ is the five dimensional standard basis vector with a 1 in the ith position, and $\boldsymbol{\Omega}_i(\boldsymbol{\rho})$ is a matrix where the element in the jth row and kth column is given by $Cov(\delta_i(\boldsymbol{s}_j), \delta_i(\boldsymbol{s}_k))$.

At the second stage of inference we use $\hat{\boldsymbol{\Theta}}$, the vector of pointwise MLEs, and $\boldsymbol{W}$ as inputs and estimate $\boldsymbol{\beta}$, A, and $\boldsymbol{\rho}$ via an iterative procedure to maximize the likelihood function. During this optimization procedure, we consider $\boldsymbol{W}$ as fixed and known, ultimately yielding estimates $\tilde{\boldsymbol{\beta}}$, $\tilde{A}$, and $\tilde{\boldsymbol{\rho}}$.

2.4 Modeling Dependence of Annual Maxima

In order to estimate the model parameters via maximum likelihood as outlined in Section 2.3, we must first select $\boldsymbol{W}$. A simple approach is to assume $\boldsymbol{\varepsilon}(\boldsymbol{s}_l)$ is independent of $\boldsymbol{\varepsilon}(\boldsymbol{s}_{l'})$ for all $l \neq l'$, resulting in a banded sparse estimator. In this work, we do not utilize this approach as it does not allow us to account for dependence between annual maxima at nearby locations. In the GC region during hurricane season, this type of dependence is anticipated; when a location is impacted by an extreme precipitation event such as a hurricane, neighboring locations will also expect see extreme levels of precipitation from the same event. An alternative approach to selecting $\boldsymbol{W}$ is to not make any assumptions on its structure, thereby allowing for dependence between annual maxima. We choose to take this approach, and estimate $\boldsymbol{W}$ via a nonparameteric block bootstrap approach; we denote this resulting estimator by $\boldsymbol{W}_{bs}$.

At station l ($l = 1, \ldots, L$), the observed series of seasonal 7-day maxima is denoted by $Y_1(\boldsymbol{s}_1), \ldots, Y_T(\boldsymbol{s}_l)$. For the bth bootstrap iteration ($b = 1, \ldots, B$), we first obtain $\{t_1^b, \ldots, t_T^b\}$, a resampled set of years chosen from $\{1, \ldots, T\}$ with replacement. We then obtain the resampled series of seasonal 7-day maxima $\boldsymbol{Y}_b^*(\boldsymbol{s}_l) = (Y_{t_1^b}(\boldsymbol{s}_l), \ldots, Y_{t_T^b}(\boldsymbol{s}_l))^T$ for $l = 1, \ldots, L$, emphasizing that for each bootstrap replication the same resampled set of years is used at all spatial locations in order to preserve the spatial dependence in the corresponding estimates. We then use numeric optimization to estimate the pointwise maximum likelihood estimates separately for each

combination of station and bootstrap replication, obtaining the matrix

$$\boldsymbol{\Gamma} = \begin{bmatrix} (\hat{\theta}_1^1(\boldsymbol{s}_1), \ldots, \hat{\theta}_1^1(\boldsymbol{s}_L), \ldots, \hat{\theta}_5^1(\boldsymbol{s}_1), \ldots, \hat{\theta}_5^1(\boldsymbol{s}_L)) \\ \vdots \\ (\hat{\theta}_1^b(\boldsymbol{s}_1), \ldots, \hat{\theta}_1^b(\boldsymbol{s}_L), \ldots, \hat{\theta}_5^b(\boldsymbol{s}_1), \ldots, \hat{\theta}_5^b(\boldsymbol{s}_L)) \\ \vdots \\ (\hat{\theta}_1^B(\boldsymbol{s}_1), \ldots, \hat{\theta}_1^B(\boldsymbol{s}_L), \ldots, \hat{\theta}_5^B(\boldsymbol{s}_1), \ldots, \hat{\theta}_5^B(\boldsymbol{s}_L)) \end{bmatrix}$$

where $\hat{\theta}_i^b(\boldsymbol{s}_l)$ is the MLE at station l based on the sample of block maxima $\mathbf{Y}_b^*(\boldsymbol{s}_l)$.

The entry in the jth row and kth column of $\boldsymbol{W}_{bs}$ is defined to be the sample covariance between the jth and kth column vectors of the matrix $\boldsymbol{\Gamma}$. This approach does allow for dependence between annual maxima at nearby locations; however, there are problems with this approach. For even a moderate number of stations, $\boldsymbol{W}_{bs}$ will be a relatively large matrix, and it is reasonable to believe that this matrix may contain at least some noise due to overfitting. Additionally, exploratory analysis indicates that $\boldsymbol{W}_{bs}$ tends to produce estimated parameter fields that are less smooth than we believe that they might be. Statistical regularization procedures have been developed to deal with these types of scenarios (Bickel et al., 2006).

Covariance tapering (Furrer et al., 2006) is a procedure that is designed to regularize covariance matrices via multiplication (using the Hadamard product) by a sparse taper matrix. Other methods of covariance regularization exist (Barnard et al., 2000; Daniels and Kass, 2001; Hannart and Naveau, 2014; Katzfuss et al., 2016; Schäfer and Strimmer, 2005); in this work we choose to regularize $\boldsymbol{W}_{bs}$ via the covariance tapering method due to the fact that the resulting matrix will be sparse, thereby eliminating long range dependence. This property is appealing in terms of being able to account for dependence between annual maxima from the same precipitation event.

We obtain the tapering based estimator of $\boldsymbol{W}$ via

$$\boldsymbol{W}_{tap}(\lambda) = \boldsymbol{W}_{bs} \circ T_{tap}(\lambda).$$

Here, $\circ$ is the Hadamard product and $T_{tap}(\lambda)$ is the taper matrix with range parameter $\lambda > 0$. Furrer et al. (2006) propose $T_{tap}(\lambda)$ to be a matrix where the jth row and kth column is given by $Cor(\|\boldsymbol{s}_j - \boldsymbol{s}_k\|)$ for any correlation function with the property that $Cor(\|\boldsymbol{s} - \boldsymbol{s}'\|) = 0 \; \forall \; \boldsymbol{s}, \boldsymbol{s}' \in \mathcal{D}$ such that $\|\boldsymbol{s} - \boldsymbol{s}'\| > \lambda$. Selecting a smaller value of λ results in a $T_{tap}(\lambda)$ that increases in terms of sparsity, which will also result in a sparse $\boldsymbol{W}_{tap}(\lambda)$. The sparsity of $\boldsymbol{W}_{tap}(\lambda)$ does not necessarily imply $Cov(\hat{\boldsymbol{\Theta}})$ will also be sparse, as evidenced by its form in (7); therefore, we do not experience any computational gains. However, this sparsity provides the intuitive appeal of avoiding the presence of dependence between annual maxima at stations that are separated by more than λ units in distance.

3 Characterizing US Gulf Coast Precipitation Extremes

We begin this section by describing the precipitation station data and GoM SST data that we use in our analysis. We then use the output of the fitted spatial model to interpolate to a grid of points covering the entire US GC region, and to characterize precipitation extremes throughout the region via a return level analysis. Next, we estimate the degree to which the Harvey event was unusual in the Houston area, and conclude by using model output to estimate exceedance probabilities throughout the region.

3.1 Data Description

In this work, the study region $\mathcal{D}$ is defined to include the portion of the US state of Texas east of the 100°W meridian, and all of the US states of Florida, Georgia, Alabama, Mississippi, and Louisiana. We use precipitation data from all Global Historical Climatology Network (GHCN) stations located in this study region; the GHCN is described in greater detail in Menne et al. (2012). As the focus of this work is on precipitation extremes during GC hurricane season (June–November), we obtain daily precipitation totals during these months for the years 1949–2017. Seasons with more than five missing values are omitted from analysis, and stations with at least 10 seasons omitted are excluded from analysis. A total of 326 stations meet these criteria and are included in analysis; their locations are plotted in Figure 1. In order to perform analysis of the Harvey as an out of sample event, data for the year 2017 are held out of the model fitting portion of the analysis.

In order to consider GoM SST as a potential covariate, we obtain a monthly mean GoM SST series by averaging all values in the Hadley Centre Sea Ice and Sea Surface Temperature (HadISST) data set (Rayner et al., 2003) between longitudes $83° - 97°$ west and latitudes $21° - 29°$ north. In this work, we wish to consider late spring GOM SST as a covariate, as this is the time frame that leads directly into hurricane season; therefore, we define our GoM SST covariate to be the average SST from March through June. Although we use the average SST from March through June in our work, exploratory analysis suggested that other similar lags may produce similar results.

The left panel of Figure 2 plots the centered and scaled GoM SST covariate, while the right panel of Figure 2 gives the corresponding histogram. The bimodal appearance of the histogram suggests that the time series tends to oscillate between low and

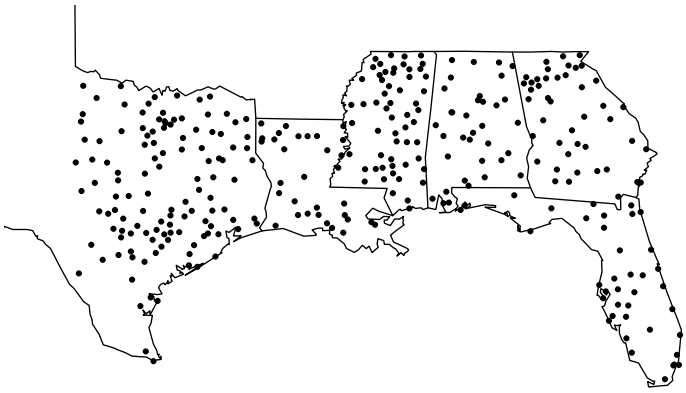

Figure 1: We plot the location of the 326 GHCN stations in the US Gulf Coast region used in this analysis.

high values. The lower mode looks to be approximately one standard deviation below the mean, and the upper mode appears to be approximately one standard deviation above the mean. Therefore, in the remainder of this work we define *low SST* and *high SST* to be a centered and scaled GoM SST value of -1 and 1 (respectively). After centering and scaling, the SST in 2017 is approximately 1.7; we refer to this GoM SST value as *2017 SST*.

3.2 Results of Spatial Analysis

For analysis, we use $\boldsymbol{W}_{tap}(\lambda)$ based on the taper matrix $T_{tap}(\lambda) = \mathbf{1}_5\mathbf{1}_5^T \otimes C_{W_2}(\lambda)$, where $C_{W_2}(\lambda)$ is a correlation matrix based on the Wendland 2 covariance function (Wendland, 1995) with $\lambda = 75$km. This choice of λ is partly based on intuition, as we believe that dependence between annual maxima due to extreme events will

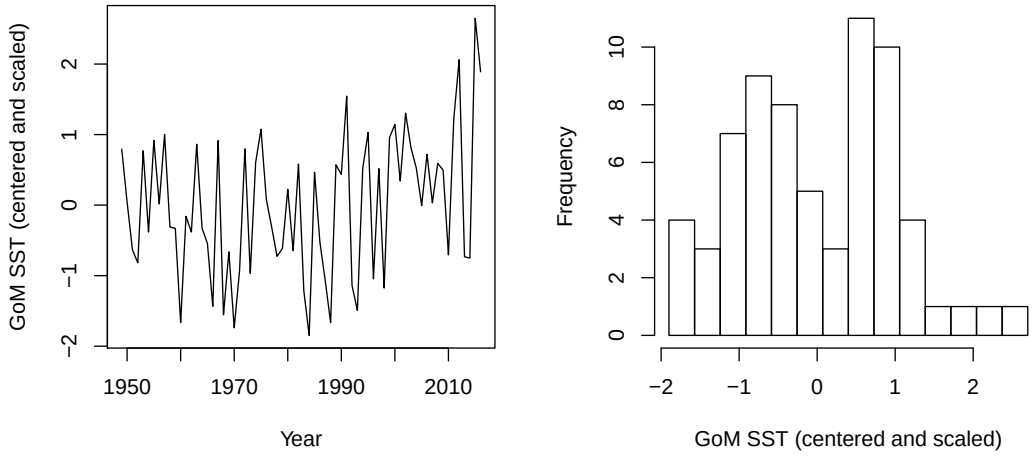

Figure 2: We center and scale the series of March – June average GoM SSTs from 1949 – 2016, and present a time series plot (L) and a histogram (R).

be localized, particularly for the GC region during hurricane season. This choice is reasonable given the physical intuition that the main reason for dependence is that a large storm can affect multiple sites simultaneously, and this is a reasonable upper bound for the physical extent of a single large precipitation event. Additionally, a sensitivity analysis indicates that the results presented here would change little for $\lambda = 150$km; beyond this distance we believe that we would be modeling more than the dependence between annual maxima due to the same event that we aim to capture. Two special cases, $\lambda \to 0$ and $\lambda \to \infty$, correspond with independent errors and absence of regularization (respectively). Through a simulation study (available in the Supplemental Materials), we explore the issue of selecting λ. The results of Simulation Study 1 suggest that the true error curve for return level estimation as a function of λ is convex, and that estimation may be improved by choosing a sensible $\lambda \in (0, \infty)$.

We also considered models without the SST covariate in the location and scale parameter (and both), but choose to use the full model specified in (3) based on AIC. Parameter estimation is performed via an iterative procedure in order to maximize the likelihood, yielding the estimates $\tilde{\boldsymbol{\beta}}$, $\tilde{A}$, and $\tilde{\boldsymbol{\rho}}$.

3.2.1 Characterizing Gulf Coast Precipitation Extremes via Return Level Estimates

To spatially interpolate the value of $\boldsymbol{\theta}(\boldsymbol{s})$ for $\boldsymbol{s} \in \mathcal{G} \subset \mathbb{Z}^2$, where $\mathcal{G}$ is a grid of points covering the US GC region, we solve the universal kriging equations (Cressie, 1993). At each $\boldsymbol{s} \in \mathcal{G}$, we obtain $\tilde{\boldsymbol{\theta}}(\boldsymbol{s})$, and use (2) to estimate 100-year return levels. Figure 3 in the Supplemental Materials presents a map of the corresponding 100-year return levels (in cm) for the three SST scenarios considered in this work; the top panel plots the estimates based on low SST, the middle panel plots the estimates based on high SST, and the bottom panel plots the estimates based on 2017 SST. We use the simulation based procedure proposed in Tye and Cooley (2015) to obtain 90% pointwise confidence intervals for each of the three SST scenarios, presented in Figure 4 in the Supplemental Materials. In the simulation based procedure, we simulate 2,500 multivariate realizations from the fitted process for all $\boldsymbol{s} \in \mathcal{G}$, and then calculate estimated 100-year return levels for each realization and use the percentile method to obtain pointwise confidence intervals.

For each of the three SST scenarios, we observe that estimated return levels tend to be higher along the Texas coast and in southern Louisiana, Mississippi, Alabama and the Florida panhandle. Both the lower and upper endpoints of the pointwise 90% confidence intervals follow a similar spatial pattern, and reflect the relatively high degree of uncertainty involved in characterizing extremes. For high SST, the estimated 100-year return levels are higher in much of the region, particularly on the

eastern Texas coastal region. The estimated 100-year return levels for 2017 SST look to be similar to high SST, and tend to show similar changes versus low SST.

Estimated 100-year return levels tend to be higher in much of the US GC for warmer SST scenarios; however, Figure 3 in the Supplementary Materials does not make it easy to quantify this effect. In order to better facilitate comparison, Figure 3 plots the ratio of estimated 100-year return levels for high SST versus low SST, and suggests that warming GoM SST does not affect the US GC region uniformly. The ratio is close to one for most of Florida and Southern Georgia, suggesting that these locations may not be impacted by GoM SSTs. In contrast, the western GC looks to be more affected by extreme precipitation events for warmer GoM SST scenarios. Figure 5 in the Supplemental Materials gives the corresponding pointwise 90% confidence intervals based on simulation based procedure, and provides additional evidence of the impact of warming GoM SSTs on extreme precipitation events on the Texas coast and southern Louisiana and Mississippi. In Figure 3, cells whose pointwise 90% confidence intervals do not contain one are denoted with a small black dot. Figure 4 plots the ratio of estimated 100-year return levels for 2017 SST versus low SST, and Figure 6 in the Supplemental Materials gives the corresponding pointwise 90% confidence intervals. The spatial pattern in these plots looks to be similar, but the impact on the western GC appears to be even greater. As before, in Figure 4, cells whose pointwise 90% confidence intervals do not contain one are denoted with a small black dot.

3.2.2 Understanding the Degree to Which Harvey was Unusual in Houston

Over the course of the Harvey event, some areas of Houston saw seven-day precipitation totals approaching 80cm. Harvey was clearly an extremely unusual precipitation

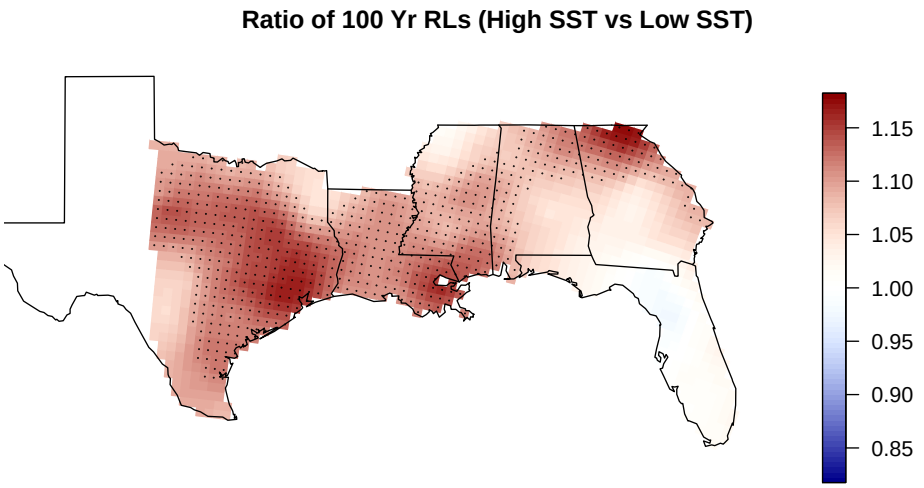

Figure 3: We plot the estimated ratio of 100-year return levels for high SST versus low SST. Cells whose pointwise 90% confidence intervals do not contain one are denoted with a small black dot.

event; the fitted model output can be used to understand just how anomalous this event was. For a range of seven-day hurricane season precipitation totals and based on output from our fitted spatial model, Figure 5 plots observed return periods in Houston for low SST, high SST, and 2017 SST (top to bottom, respectively). In this analysis, the observed return period is defined to be the reciprocal of estimated exceedance probability. We plot pointwise 90% confidence intervals, shown in gray, that are generated via the simulation based approach. Although there is a great deal of uncertainty, these graphs suggest that devastating precipitation events during hurricane season in Houston are more unusual when the GoM SST is low and less unusual when the GoM SST is higher.

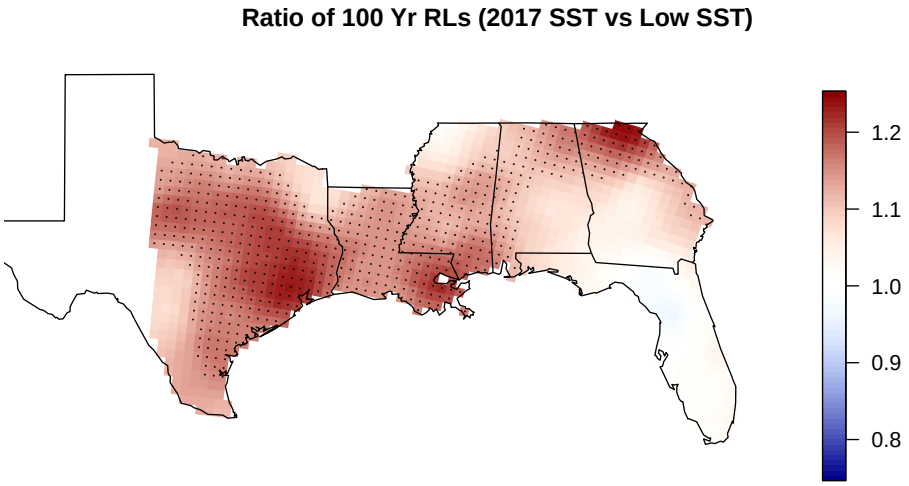

Figure 4: We plot the estimated ratio of 100-year return levels for 2017 SST versus low SST. Cells whose pointwise 90% confidence intervals do not contain one are denoted with a small black dot.

3.2.3 Estimating the Chances of Observing another Harvey-level Event in the Gulf Coast Region

In terms of estimating precipitation return periods for the Harvey event in Houston, Emanuel (2017) considers a storm total of 50 cm, noting that it is a "conservative value". Risser and Wehner (2017) spatially average station data over a larger and a smaller region surrounding Houston. They find that area averaged storm total is approximately 48 cm in their larger region, and the corresponding total is approximately 70 cm in their smaller region. Although parts of Houston may have experienced higher seven-day precipitation totals due to Hurricane Harvey, we consider precipitation totals of 50 cm and 70 cm in this portion of the analysis.

Based on output from our fitted model, Figure 6 plots the estimated probability of observing a seven-day hurricane season precipitation total in excess of 50 cm for

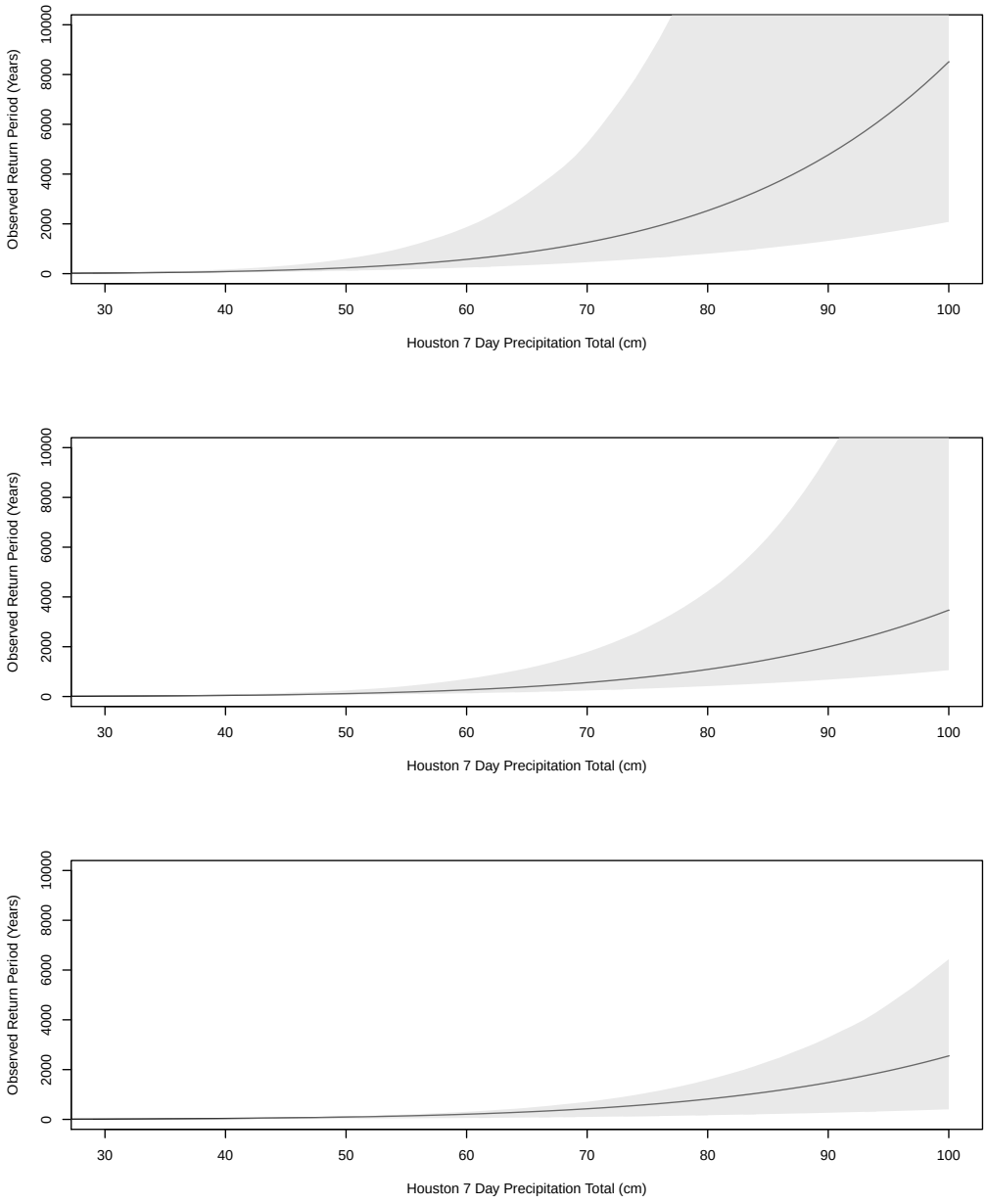

Figure 5: For a range of seven-day hurricane season precipitation totals (in cm) and based on output from our fitted spatial process, we plot observed return periods (reciprocal of estimated exceedance probabilities) in Houston for low SST (top panel), high SST (middle panel), and 2017 SST (bottom panel). Pointwise 90% confidence intervals (shown in gray) are generated via the simulation based approach.

low SST, high SST, and 2017 SST in the GC region. The western GC has the highest estimated exceedance probabilities, and these estimates tend to be larger for warmer GoM SST. Another way to estimate the probability of observing another event on the scale of Harvey is to consider annual average precipitation as a baseline. The seven-day total of 50 cm in Houston roughly corresponds to 38% of its average annual precipitation. Figure 7 plots the estimated probability of observing a seven-day hurricane season precipitation total in excess of 38% of each location's annual average precipitation for low SST, high SST, and 2017 SST. It is interesting to note the differences between Figure 6 and 7. The probability of exceeding 50 cm of precipitation in coastal Texas increase as GoM SST increases, but the estimated probability is close to zero in areas away from the central and western GC. When annual average precipitation is taken into account, the estimated exceedance probabilities tend to be higher in southern and central Texas. Figures 7 and 8 in the Supplemental Materials are analogous to Figures 6 and 7, differing only in that they consider a storm total of 70cm, and yield similar conclusions.

Looking at exceedance probabilities in this manner offers two unique viewpoints. The approach in Figure 6 provides estimates of exceeding a extremely large absolute amount of precipitation; the approach in Figure 7 provides estimates of exceeding a large amount of precipitation relative to each location's climate. Both perspectives may be important in terms of informing engineering standards, and when used together could offer a more complete picture of precipitation extremes at GC locations.

4 Discussion

In this work, we assume that seven-day maximum precipitation totals during hurricane season at GC locations are approximately GEV, where the location and scale

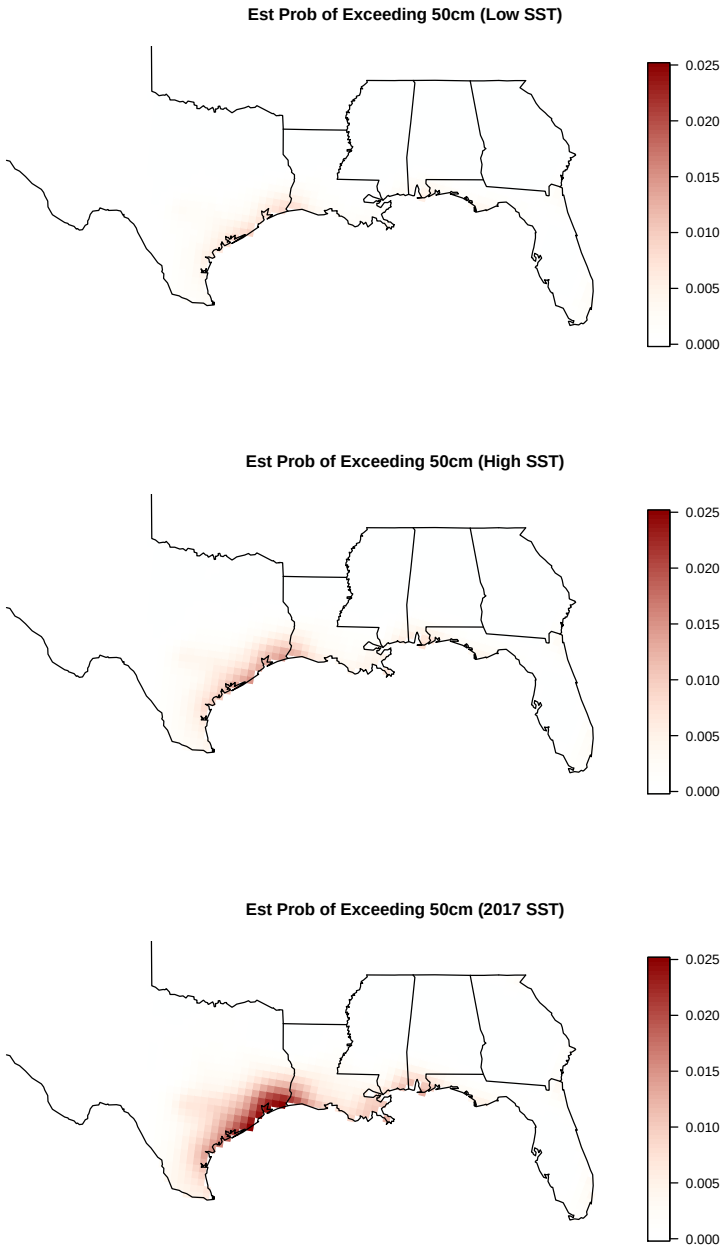

Figure 6: Based on output from our fitted model, we plot the estimated probability of observing a seven-day hurricane season precipitation total in excess of 50 cm for low SST (top panel), high SST (middle panel), and 2017 SST (bottom panel).

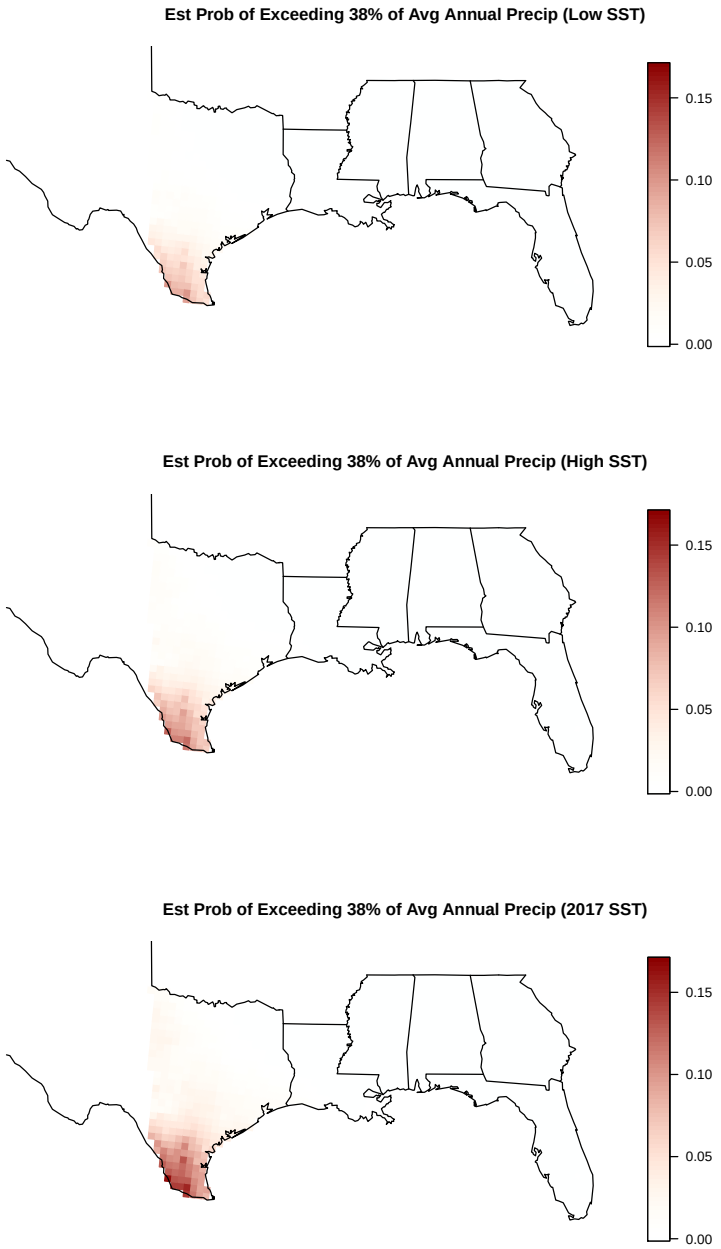

Figure 7: Based on output from our fitted model, we plot the estimated probability of observing a seven-day hurricane season precipitation total in excess of 38% of each location's annual average precipitation (corresponding to 50 cm in Houston) for low SST (top panel), high SST (middle panel), and 2017 SST (bottom panel).

parameters are allowed to depend on a late spring GoM SST covariate. Our analysis uses precipitation data from the GHCN, and a GoM SST covariate derived from the HadISST data set. To model the GEV parameters, we use a multivariate spatial model and perform inference using a two-stage frequentist approach, where pointwise MLEs are used to estimate parameters of the spatial process. In order to characterize precipitation extremes across the region, we use universal kriging to perform spatial interpolation. The analysis presented in Section 3 indicates that warmer late spring GoM SSTs correspond with higher seven-day precipitation extremes during hurricane season in the western US GC. This increase seems to be the largest in the eastern Texas coastal region and southern Louisiana.

Generally speaking, the method proposed in this work could be compared with two broad classes of methods in terms of aims and research objectives. The Bayesian hierarchical approach to modeling the GEV parameters may be an appealing alternative, as it eliminates the need for two-stage analysis; however, dependence between observations would need to be captured by somehow introducing dependence on the latent structure. Our method has more in common with works that have used two-stage frequentist approaches to spatial analysis. However, other works of this type have not attempted to model dependence between annual maxima as we have. Our procedure of modeling this type of dependence using a regularized bootstrap based estimator is novel, and a simulation study (available in the Supplemental Materials) suggests that it may yield better return level estimates for an appropriate choice of λ.

Although we only consider precipitation extremes in this work, the methodology proposed here could be applied to other types of data. In terms of environmental applications, this method might be useful for modelling air pollution, air temperature, and wind speed. However, when using this procedure for other types of data, the

analyst would need to think carefully about a reasonable value of λ, as the choice would be closely tied to the inherent dependence structure for that data type.

Alexander et al. (2018) study SSTs in large marine ecosystems (LME) throughout the northern hemisphere and use climate model output to predict changes in SST. In the GoM, Alexander et al. (2018) indicate that the increase in SST could be in the range of $0.2°\text{C} - 0.4°\text{C}$ per decade over the years $1976 - 2099$. The authors also predict that GoM SSTs may continue to exhibit similar amounts of year to year variability, suggesting that the time series of late spring GoM SSTs may continue to oscillate as depicted in Figure 8. Alexander et al. (2018) write that, "The shift in the mean was so large in many regions that SSTs during the last 30 years of the $21st$ century will always be warmer than the warmest year in the historical period". In their work, the authors define the historical period to be $1976 - 2005$.

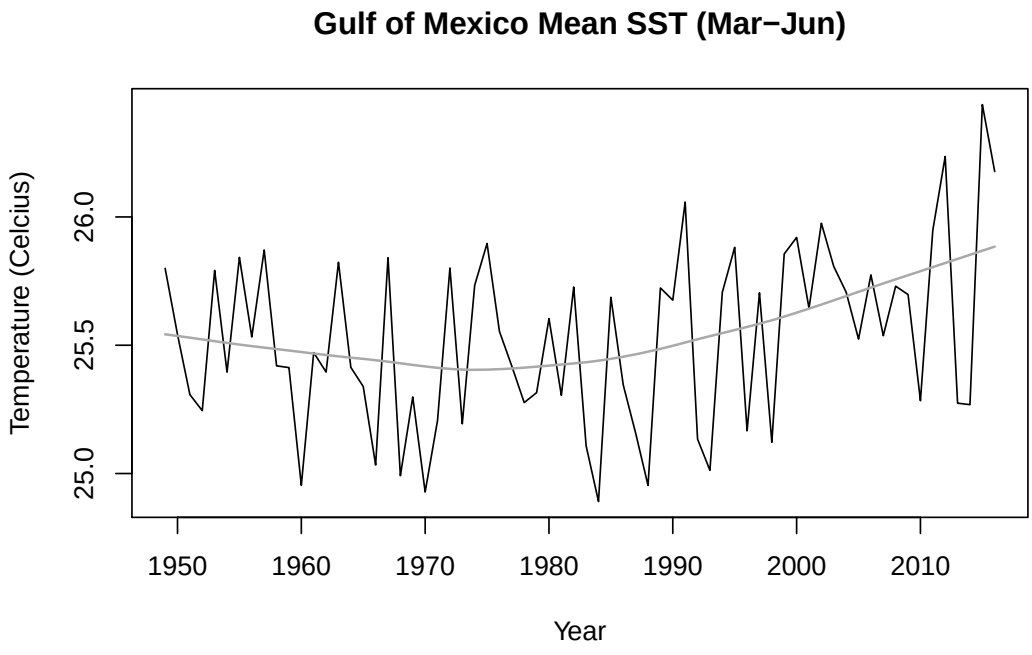

Figure 8: We plot the time series of late spring mean GoM SSTs.

If the GoM SST increases predicted by Alexander et al. (2018) come to fruition, even the coolest GoM SST seasons during the last 30 years of this century could result in a 10% to 20% increase in 100-year precipitation return levels during hurricane season for the western GC region compared to present day cool seasons. In particular, residents of Houston and New Orleans, who have experienced devastating hurricanes in recent history, may experience more intense precipitation extremes as a result of warming SSTs.

Supplemental Materials

Additional information and supporting material for this article is available online at the journal's website.

Data Availability Statement

The data used in this analysis are publicly available via `ftp://ftp.ncdc.noaa.gov/pub/data/ghcn/daily/`.

Acknowledgements

This material was based upon work partially supported by the National Science Foundation under Grant DMS-1638521 to the Statistical and Applied Mathematical Sciences Institute. Any opinions, findings, and conclusions or recommendations expressed in this material are those of the author(s) and do not necessarily reflect the views of the National Science Foundation.

Clemson University is acknowledged for its generous allotment of computing time

on the Palmetto Cluster. Mark Risser was supported by the Director, Office of Science, Office of Biological and Environmental Research of the U.S. Department of Energy under Contract No. DE-AC02-05CH11231. Ken Kunkel was supported by NOAA through the Cooperative Institute for Climate and Satellites - North Carolina under Cooperative Agreement NA14NES432003.

References

Alexander, M. A., Scott, J. D., Friedland, K. D., Mills, K. E., Nye, J. A., Pershing, A. J., and Thomas, A. C. (2018). Projected sea surface temperatures over the 21st century: Changes in the mean, variability and extremes for large marine ecosystem regions of Northern Oceans. *Elem Sci Anth*, 6(1).

Barnard, J., McCulloch, R., and Meng, X.-L. (2000). Modeling covariance matrices in terms of standard deviations and correlations, with application to shrinkage. *Statistica Sinica*, pages 1281–1311.

Bickel, P. J., Li, B., Tsybakov, A. B., van de Geer, S. A., Yu, B., Valdés, T., Rivero, C., Fan, J., and van der Vaart, A. (2006). Regularization in statistics. *Test*, 15(2):271–344.

Brown, B. M. and Resnick, S. I. (1977). Extreme values of independent stochastic processes. *Journal of Applied Probability*, 14(4):732739.

Coles, S. G. (2001). *An Introduction to Statistical Modeling of Extreme Values*. Springer Series in Statistics. Springer-Verlag London Ltd., London.

Cooley, D., Cisewski, J., Erhardt, R. J., Jeon, S., Mannshardt, E., Omolo, B. O., and Sun, Y. (2012). A survey of spatial extremes: measuring spatial dependence and modeling spatial effects. *Revstat*, 10(1):135–165.

Cooley, D., Nychka, D., and Naveau, P. (2007). Bayesian spatial modeling of extreme precipitation return levels. *Journal of the American Statistical Association*, 102(479):824–840.

Cooley, D. and Sain, S. R. (2010). Spatial hierarchical modeling of precipitation

extremes from a regional climate model. *Journal of agricultural, biological, and environmental statistics*, 15(3):381–402.

Cressie, N. (1993). *Statistics for Spatial Data*. John Wiley & Sons, Inc.

Daniels, M. J. and Kass, R. E. (2001). Shrinkage estimators for covariance matrices. *Biometrics*, 57(4):1173–1184.

Davison, A. C., Padoan, S. A., and Ribatet, M. (2012). Statistical Modeling of Spatial Extremes. *Statistical Science*, 27(2):161–186.

Dyrrdal, A. V., Lenkoski, A., Thorarinsdottir, T. L., and Stordal, F. (2015). Bayesian hierarchical modeling of extreme hourly precipitation in Norway. *Environmetrics*, 26(2):89–106.

Emanuel, K. (2017). Assessing the present and future probability of Hurricane Harvey's rainfall. *Proceedings of the National Academy of Sciences*, 114(48):12681–12684.

Finley, A. O., Banerjee, S., Ek, A. R., and McRoberts, R. E. (2008). Bayesian multivariate process modeling for prediction of forest attributes. *Journal of Agricultural, Biological, and Environmental Statistics*, 13(1):60–83.

Furrer, R., Genton, M. G., and Nychka, D. (2006). Covariance tapering for interpolation of large spatial datasets. *Journal of Computational and Graphical Statistics*, 15(3):502–523.

Gaetan, C. and Grigoletto, M. (2007). A hierarchical model for the analysis of spatial rainfall extremes. *Journal of Agricultural, Biological, and Environmental Statistics*, 12(4):434–449.

Ghosh, S. and Mallick, B. K. (2011). A hierarchical Bayesian spatiotemporal model for extreme precipitation events. *Environmetrics*, 22(2):192–204.

Hannart, A. and Naveau, P. (2014). Estimating high dimensional covariance matrices: A new look at the Gaussian conjugate framework. *Journal of Multivariate Analysis*, 131:149–162.

Holland, D. M., Caragea, P., and Smith, R. L. (2004). Regional trends in rural sulfur concentrations. *Atmospheric Environment*, 38(11):1673–1684.

Holland, D. M., De, O. V., Cox, L. H., and Smith, R. L. (2000). Estimation of regional trends in sulfur dioxide over the Eastern United States. *Environmetrics*, 11(4):373–393.

Kabluchko, Z., Schlather, M., and De Haan, L. (2009). Stationary max-stable fields associated to negative definite functions. *The Annals of Probability*, 37(5):2042–2065.

Katzfuss, M., Stroud, J. R., and Wikle, C. K. (2016). Understanding the ensemble kalman filter. *The American Statistician*, 70(4):350–357.

Menne, M. J., Durre, I., Vose, R. S., Gleason, B. E., and Houston, T. G. (2012). An overview of the global historical climatology network-daily database. *Journal of Atmospheric and Oceanic Technology*, 29(7):897–910.

Opitz, T. (2013). Extremal t processes: Elliptical domain of attraction and a spectral representation. *Journal of Multivariate Analysis*, 122:409 – 413.

Rayner, N., Parker, D., Horton, E., Folland, C., Alexander, L., Rowell, D., Kent, E., and Kaplan, A. (2003). Global analyses of sea surface temperature, sea ice,

and night marine air temperature since the late nineteenth century. *Journal of Geophysical Research: Atmospheres*, 108(D14).

Ribatet, M. and Sedki, M. (2013). Extreme value copulas and max-stable processes. *Journal de la Socit Franaise de Statistique*, 153(3):138–150.

Risser, M. D. and Wehner, M. F. (2017). Attributable human-induced changes in the likelihood and magnitude of the observed extreme precipitation during Hurricane Harvey. *Geophysical Research Letters*, 44(24):12457–12464.

Russell, B. T., Cooley, D. S., Porter, W. C., and Heald, C. L. (2016). Modeling the spatial behavior of the meteorological drivers' effects on extreme ozone. *Environmetrics*, 27(6):334–344. env.2406.

Sang, H. and Gelfand, A. E. (2009). Hierarchical modeling for extreme values observed over space and time. *Environmental and Ecological Statistics*, 16(3):407–426.

Schäfer, J. and Strimmer, K. (2005). A shrinkage approach to large-scale covariance matrix estimation and implications for functional genomics. *Statistical applications in genetics and molecular biology*, 4(1).

Schlather, M. and Tawn, J. A. (2003). A dependence measure for multivariate and spatial extreme values: Properties and inference. *Biometrika*, 90(1):139–156.

Schliep, E. M., Cooley, D., Sain, S. R., and Hoeting, J. A. (2010). A comparison study of extreme precipitation from six different regional climate models via spatial hierarchical modeling. *Extremes*, 13(2):219–239.

Smith, R. L. (1990). Max–stable processes and spatial extremes. *Unpublished manuscript*, 205.

Trenberth, K. E., Cheng, L., Jacobs, P., Zhang, Y., and Fasullo, J. (2018). Hurricane Harvey links to ocean heat content and climate change adaptation. *Earth's Future*, 6.

Tye, M. R. and Cooley, D. (2015). A spatial model to examine rainfall extremes in Colorado's Front Range. *Journal of Hydrology*, 530(Supplement C):15 – 23.

van Oldenborgh, G. J., van der Wiel, K., Sebastian, A., Singh, R., Arrighi, J., Otto, F., Haustein, K., Li, S., Vecchi, G., and Cullen, H. (2017). Attribution of extreme rainfall from Hurricane Harvey, August 2017. *Environmental Research Letters*, 12(12):124009.

Wackernagel, H. (2003). *Multivariate Geostatistics*. Springer Science & Business Media.

Wendland, H. (1995). Piecewise polynomial, positive definite and compactly supported radial functions of minimal degree. *Advances in Computational Mathematics*, 4(1):389–396.